Flow and Leakage Characteristics in Sealing Chamber of a Variable Geometry Hypersonic Inlet

XIA Feng[1], *SUN Bo*[1*], *YU Jianyi*[2], *YUE Lianjie*[3], *GAO Yu*[1], *DAI Chunliang*[1]

1. College of Mechanical Engineering, Nanjing University of Science and Technology, Nanjing 210094, P. R. China;
2. Beijing System Design Institute of Electro-mechanic Engineering, Beijing 100190, P. R. China;
3. State Key Laboratory of High-Temperature Gas Dynamics, Beijing 100190, P. R. China

(Received 15 October 2022; revised 20 November 2022; accepted 10 December 2022)

Abstract: When the variable geometry hypersonic inlet is sealed with ceramic wafers, the cavity flows inside the sealing chamber can be affected by the boundary layer near the side wall. To study the influence of the boundary layer thickness near the side wall on the flow and leakage characteristics in sealing chamber, the numerical calculation of the cavity flow in the sealing chamber under different inflow boundary layer thicknesses is carried out. The results show that three-dimensional cavity flow structures are close to being asymmetric, and the entrance pressure of the leakage path can also be affected by asymmetry; with the increase of the thickness of the boundary layer, the pressure at the cavity floor and the seal entrance decreases. Finally, the existing leakage prediction model is modified according to the distribution rule of the cavity floor and the flow properties in the leakage path.

Key words: variable geometry inlet; ceramic wafer seal; vortex structure; leakage rate; asymmetry three-dimensional cavity flow

CLC number: V211.3 **Document code:** A **Article ID:** 1005-1120(2022)06-0663-09

0 Introduction

Hypersonic vehicles need to be used adjustable flow channels to meet the engine requirements of extending the operating range of flight Mach number. For the sake of smooth adjustment, there will be a gap between the movable panel and the side wall of the inlet. Under the hypersonic flight condition, the high-temperature gas will flow into the equipment cabin through this gap, causing the failure of electronic components, and even leading to equipment damage. High-temperature dynamic structural seals are required to seal this gap[1-3], which can provide the sealing performance while considering the normal operation of the regulating system. As a commonly used dynamic sealing material, the ceramic wafer has advantages of small specific gravity, high melting point, high hardness, good chemical stability, corrosion resistance, etc. It can ensure the normal operation of the variable geometry inlet when limiting leakage and insulating heat.

At present, the common sealing methods in the aerospace field are labyrinth sealing and other rotary sealing to reduce the leakage of the working medium in the engine[4-5]. Ceramic wafer seal is often used in the connection parts of various cabin sections, the control rudder shaft, and the movable engine panel. Steinetz[6] proposed the sealing method and the corresponding leakage model, and verified the effectiveness of the seal and the accuracy and scope of application of the calculation model through the experimental research. Ceramic wafer seals were first used in the X-51 scramjet engine. The high-temperature and high-pressure environment (1 373—1 640 K, 0.7 MPa) at the engine sealing position has brought great challenges to the seals. In the meantime, the seals also need to have strong anti-oxidation and friction resistance capabilities to en-

*Corresponding author, E-mail address: hypersun@126.com.

How to cite this article: XIA Feng, SUN Bo, YU Jianyi, et al. Flow and leakage characteristics in sealing chamber of a variable geometry hypersonic inlet[J]. Transactions of Nanjing University of Aeronautics and Astronautics, 2022, 39(6): 663-671.
http://dx.doi.org/10.16356/j.1005-1120.2022.06.003

sure that they still adhere to the side wall after withstanding the thermal cycle.

The existing work on dynamic structural seals mainly focuses on sealing materials. The relevant performance parameters of the ceramic wafer are obtained through high-temperature thermal tests and the sealing reliability is analyzed. The leakage characteristics of the dynamic seal are rarely analyzed from the perspective of the cavity flow. In this paper, for the background of variable geometry hypersonic inlet, a seal structure model is established to study the flow properties and leakage laws in the sealing chamber by means of a numerical simulation method.

Fig.1 shows the inner sealing structure of an inlet. When the gap is sealed with a ceramic wafer, a cavity structure is formed above the sealing chamber. The internal static gas is driven by the high-speed incoming flow of the inlet to form a cavity flow[7-8], which is similar to the combined flow of the front and backward-facing steps. The cavity flow inside the sealing chamber can be changed by the boundary layer of the leading edge and side wall at the same time, and the flow properties are different from the typical three-dimensional cavity flow[9-10]. In the cavity flow, the fit tolerance between the ceramic wafer and the seal cavity results in two leakage channels around the seal; namely, the first leakage path between the ceramic wafer and the side wall, and the second leakage path formed between the wafer and the top surfaces. The rear of the wafer is an inclined coil spring structure, which aims to provide the sealing preload by utilizing the spring back performance of the spring.

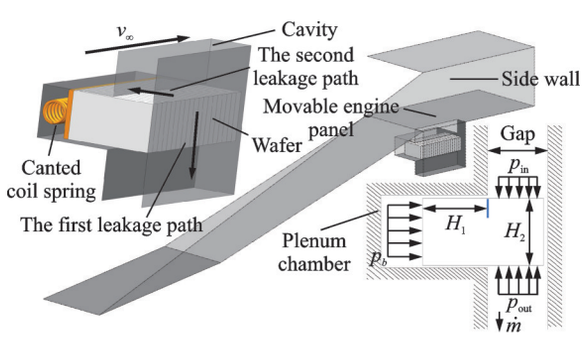

Fig.1 Sealing structure of the inlet

When the gas in the cavity flows through both sides of the cavity floor, it flows into the equipment cabin through the leakage path. Because the width of the leakage channel is much narrower than the sealing gap, the internal flow is the laminar flow between two nonslip parallel plates, which is directly affected by the pressure and temperature distribution generated by the cavity flow upstream on both sides of the floor. Also, leakage flow has little effect on the cavity flow. Therefore, the cavity structure and the seal can be separated. The flow characteristics in the cavity can be studied first, and then its influence on the leakage law can be explored.

1 Numerical Method

Because of the transonic flow in the cavity caused by the supersonic entrance, the three-dimensional compressible Navier-Stokes equations are solved to simulate the cavity flow inside the sealing chamber. Since it has advantages of low numerical dissipation and high resolution, Roe-FDS (Flux-difference splitting) scheme is used to discretize the convective flux. Time discretization using an implicit scheme and the turbulence model is two k-ω SST.

Figs.2(a, b) show the flow model of the side wall cavity and the computational grid. The cavity structure parameter: The ratio of length to width is 8∶1, and the ratio of depth to width is 3∶1. Therefore, the narrow cavity should experience an open-type flow field. The grid near the inner wall of the cavity and the side plate is densified, and the grid amount in the cavity is 860 000, accounting for 40% of the total. $y^+<1$ meets the k-ω requirements of the SST turbulence model near the wall.

Fig.2(c) shows the cavity and seal structure grid, the mesh nodes distribution above the seal is consistent with that in Fig.2(a) to ensure that the external flow field is not interfered with by grid factors during the comparative analysis of the calculation results.

Considering the application background in the variable geometry inlet, the inflow condition is set as follows: Mach=4.5, incoming static pressure

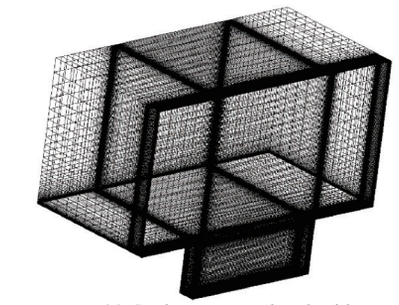

(a) Cavity computational grid

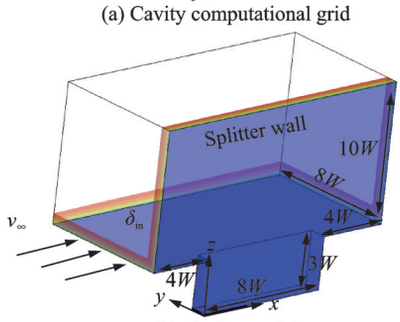

(b) Cavity model

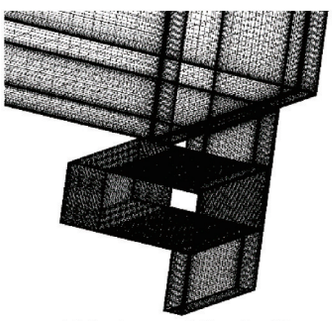

(c) Seal computational grid

Fig.2 Model and mesh structure

p_∞=11 000 Pa, and static temperature T_∞=360 K. The entrance velocity distribution is given to control the thickness of the incoming boundary layer. Because of the interaction between the side plate and the leading edge, both of them need to give the boundary layer thickness together. Therefore, the distance between the grid point and the wall surface is obtained by indexing all grid points at the entrance boundary through the judgment function δ_l. And, the velocity distribution is given in combination with the 1/7 power law[11].

$$v=\begin{cases} v_\infty(\delta_l/\delta_{in})^{1/7} & 0<\delta_l<\delta_{in} \\ v_\infty & \text{else} \end{cases} \tag{1}$$

$$\delta_l=\min(\delta_x,\delta_y) \tag{2}$$

where δ_{in} is the boundary layer thickness, which is set as $0.2W$ (width of the cavity), $0.6W$, and $1.0W$, respectively to simulate the cavity flow under different boundary layer thicknesses.

Steinetz[6] proposed a semiempirical formula for predicting the leakage rate of ceramic wafer seals. To study the influence of flow factors on the leakage characteristics, the factors causing the change of the leakage characteristics are omitted, due to the deformation of the seal structure caused by high temperature and pressure. Therefore, the test data correction part in the formula is dropped, and only the theoretical derivation part is reserved. The seal leakage rate per unit length is

$$\dot{m}/L=\frac{(p_{in}^2-p_{out}^2)}{24\mu RT}\left(\frac{h_1^3}{H_1}+\frac{h_2^3}{H_2}\right) \tag{3}$$

where p_{in} and p_{out} are the inlet and outlet pressures of the sealing structure, respectively; h_1 and h_2 the leakage path widths between the wafer, the top plate, and the side wall; and H_1 and H_2 the lengths of the two leakage paths. In Eq.(3), the gas in the leakage channel is supposed to be isothermal, and the change of pressure along the sealing direction is ignored. Therefore, the formula only can apply to the situation where the temperature is litter change, and the leakage inlet pressure is evenly distributed along the flow direction. To apply the leakage prediction in the variable geometry inlet, the sealing model is modified based on the study of the flow properties and pressure distribution of the sealing chamber.

2 Validation

The experimental cavity flow database provided by Ref.[12] is used for validation. The ratio of the length, width and depth of the cavity structure in the selected test sample is $L:W:D$=8:5:1. The inflow condition is set as follows: Mach=1.5; Re (Reynolds number per unit length)=2×10^6/ft, p=13 408 Pa, and T=224.13 K. Fig.3 shows the comparison between the numerical simulation and experiment date of the pressure coefficients on the centerline of the leading edge, front wall, floor, rear wall, and rear edge of the cavity. It can be seen that the difference between those two results is minimal, especially in the part of the rear wall and the rear edge. The maximum pressure error is 7%, and the

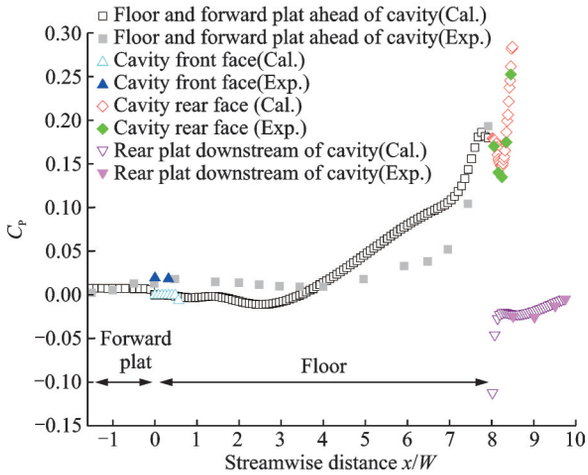

Fig.3 Comparison of pressure coefficients

overall pressure coefficient distribution trend is the same, which indicates that the calculation method can satisfactorily simulate the pressure distribution on the cavity floor.

3 Results and Analysis

3.1 Flow structure within the cavity

Fig.4 shows the flow structure with the new Omega criterion[13] and pressure contour, where the thickness of the incoming boundary layer is $1.0W$. The leading-edge vortex nears the front wall of the cavity in Fig.4. The front corner vortex is located at the junction of the front wall and the floor of the cavity. The front vortex is located on the right side of both two vortices. Occupying the middle to the back half of the cavity is a recirculation zone, which is the defining feature of an open-type cavity flow[14]. The impinging of the shear layer on the rear wall occurs near the top of the cavity ($z/W \approx 2.94$—2.95),

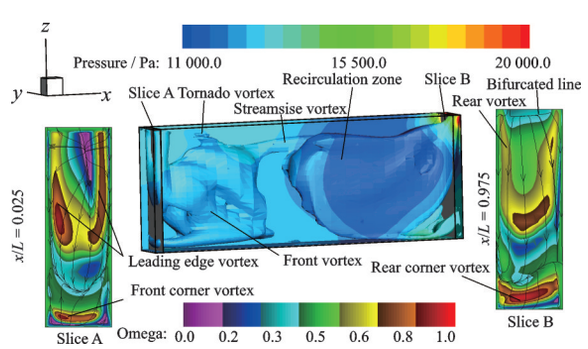

Fig.4 New Omega criterion iso-surface (Omega=0.52) colored with pressure

and the presence of bifurcation lines at the same locations in slice B is evidence of flow separation. The flow above the bifurcated line leaves the cavity upward, while the flow below the bifurcated line flows downward along the rear wall, and flows in the reverse direction at the corner of the rear wall. During the return process, the flow gradually rises upward until it joins the shear layer and enters the recirculation vortex along the flow direction. The higher separation point of the shear layer allows the recirculation zone to almost fill the second half of the cavity. The structure of the trailing edge vortex near the rear wall of the cavity at the outside of the recirculation zone is similar to that of the leading-edge vortex, and the same similarity is found between the rear corner vortex and the front corner vortex. Different from these vortices close to the center plane of the cavity or symmetrically on both sides of the cavity, the single tornado[15] vortex and streamwise vortex appear near the sidewall, which indicates that the flow in the cavity is asymmetric.

Fig.5 shows the streamlines within the cavity for the x-z plane at $y/d=0.02$, $y/d=0.5$, and $y/d=0.98$ in the three cases (case 1: $\delta_{in}=0.2W$; case 2: $\delta_{in}=0.6W$; case 3: $\delta_{in}=1.0W$). From all three cases, significant differences can be found in the flow characteristics of the front vortex in three different x-z planes. Compared with the obvious vortex structure in the central plane, there is no sign of the existence of any front vortex at the same position on the far side of the wall ($y/d=0.98$), which is replaced by a convergence line.

The direction of rotation of the front vortex and the front corner vortex below causes the flow to enter the recirculation zone along the convergence line, which is the main source of mass in the recirculation zone. The mass flowing into the recirculation zone is transported from the position far away from the side wall to the position near the side wall in a lateral movement and then flows into the front vortex to complete the cycle.

Compared with Figs.5(a2, b2, c2), it can be found that while the thickness of the boundary layer

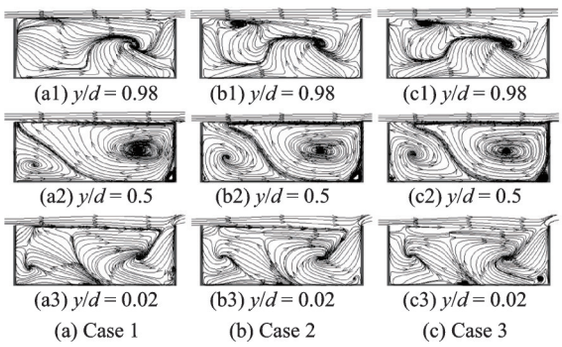

Fig.5 Streamlines in the x-z plane of cases 1, 2 and 3

increases, the space occupied by the front corner vortex in the front half of the cavity expands continuously. The position of the leading edge vortex also rises with the contact line between the front corner vortex and the front vortex. The vortex structure in the cavity exhibits a tendency to extrude toward the shear layer.

3.2 Summary of flow structure in the sealing chamber

Fig.6(a) shows the streamlines in the y-z plane at $x/W=4$ of the sealing chamber, from which the combination of leakage and cavity flow can be observed. The vortex core near the wall corresponds to the streamwise vortex in Fig.2. Driven by the pressure difference between the outlet and the bottom of the cavity, the gas escapes through two leakage paths. The plenum chamber exists to preserve the deformation space of the spring that causes the fluid through the second leakage path to gather there. The upstream and downstream of the chamber correspond to the inflow and outflow sections of the second leakage path respectively. From Fig. 6 (b), it can be found that the pressure distribution in the outflow section is consistent along the transverse direction of the y-axis. Compared with the first leakage path, the outlet section of the second leakage path shows excellent two-dimensional properties, which is entirely due to the cushioning characteristics of the plenum chamber.

Through previous research, Fig.7 shows the graphical representation of the vortex structure and streamlines in the sealing chamber.

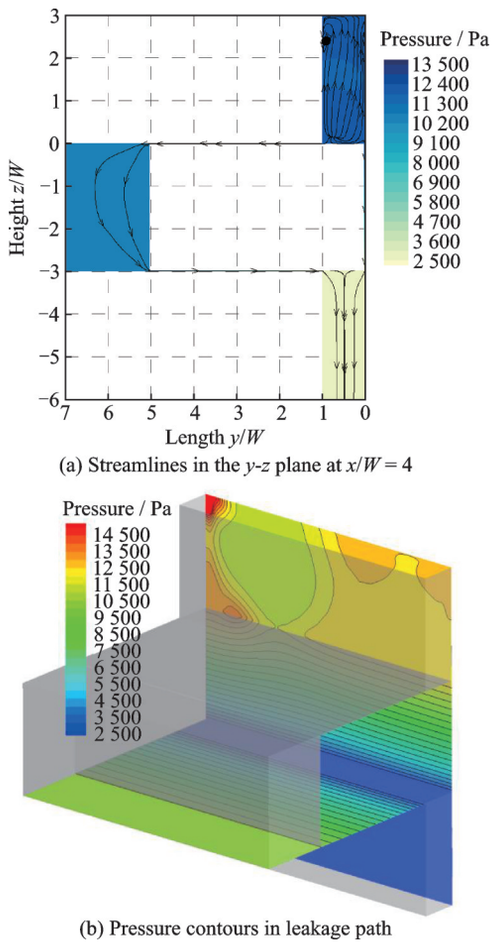

Fig.6 Pressure contours in the sealing chamber

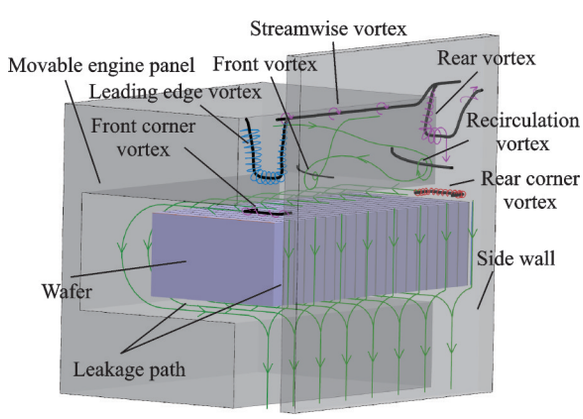

Fig.7 Diagrammatic summary of the flow streamlines and vortex structure in an open-type cavity with L: D: W=8:3:1

3.3 Cavity floor pressure distribution

Fig.8(a) shows the pressure coefficient distribution of the cavity floor of the three cases. All these results indicate that the pressure coefficient decreases gradually from the front end, and the relatively sparse contour distribution indicates that the

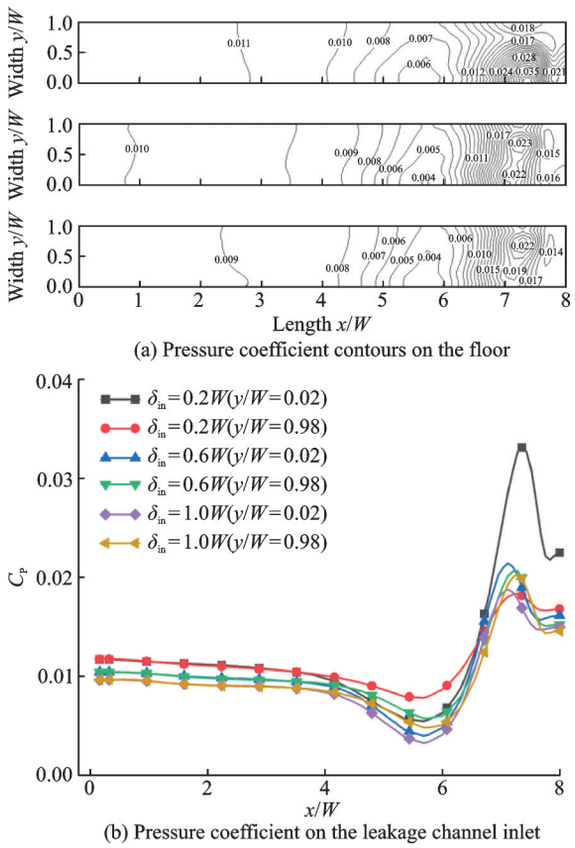

Fig.8 Pressure coefficient on the floor of cavity

fluid velocity above this region ($x/W<4$) is devoid of any high-speed flow structures. In the ($x/W \approx 5$—6) section, the pressure coefficient reduces to the minimum, which appears near the side wall. The pressure coefficient rises rapidly in the latter half of the bottom section ($x/W \approx 6$—8), and the dense pressure contour distribution indicates that the shear layer fluid flows downward along the back wall of the cavity at this position. By comparing the positions of the maximum of the three cases, it can be found that with the increase of the boundary layer thickness, the maximum offsets away from the side wall. The momentum in the shear layer decreases as the boundary layer increases and the flow near the bottom plate approaches stagnation, which leads to a decrease in the total pressure coefficient in Fig.8 (a). The pressure coefficient curves in Fig.8(b) are on both sides of the floor. The location near the side wall is $y/W=0.02$, and the location far from the wall is $y/W=0.98$, corresponding to the entrance of the first and second leakage paths, respectively. In the front section ($x/W=0$—3.8), the pressure coefficient on both sides is consistent and decreases linearly. However, in the bottom half of the floor, the maximum pressure coefficient moves away from the side wall with the increase of the thickness of the boundary layer, making the maximum value of the far wall side in case 3 exceed the near wall side, while the overall pressure coefficient decreases, causing the pressure coefficient of the near wall side in case 1 to be far greater than that in other examples.

The leakage prediction formula proposed by Steinetz is derived from the non-slip flat plate laminar flow under isothermal conditions. Besides, it is considered that the seal inlet pressure is equal to the back pressure and is evenly distributed. The change in the leakage amount is a linear growth process when it increases along the seal length. For the above reasons, the formula can be used under the following conditions

$$\frac{\partial^2 p^2}{\partial y^2}=C;\frac{\partial p}{\partial x}=0 \tag{4}$$

Therefore, the distribution of parameter p^2 is an important basis for calculating leakage. Fig.9 shows the square of pressure as the function of leakage distance. In the result of $x/W=1$ (at the first leakage path) and $x/W=4$ (at the second leakage path), the square of pressure decreases linearly in the leakage path. Curves ($x/W=7.2$ and $x/W=5.8$) represent the maximum and minimum positions in Fig.8(b), respectively, which shows a parabolic trend at the inlet of the leakage channel, but it still reduces linearly at the outlet.

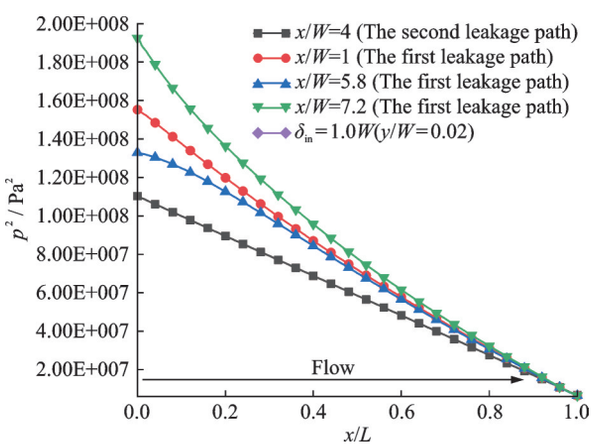

Fig.9 Square of pressure in leakage channel

3.4 Modification of leakage calculation model

The non-uniform pressure distribution at the entrance of the leakage channel under the influence of cavity flow makes Steinetz's computational model not completely applicable. Therefore, the model is modified through the research in the previous section.

Because the square of pressure decreases linearly in the outflow section of the second leakage path and the first half of the first leakage path

$$\frac{\partial^2 p^2}{\partial y}=C \tag{5}$$

which meets the requirement of Eq.(4), furthermore. Taking the inlet and outlet parameters of the outflow section into Eq.(3) yields

$$\dot{m}/L=\frac{p_b^2-p_{out}^2}{24\mu RT}\frac{h_2^3}{H_2} \tag{6}$$

The pressure in the outflow section is evenly distributed along the sealing direction. Considering that the mass flow rates of the inflow section and the outflow section are equal, it is completely feasible to calculate the leakage rate in the second leakage path through the outflow section

$$m_2=\frac{p_b^2-p_{out}^2}{24\mu RT_b}\frac{h_2^3 l}{H_2} \tag{7}$$

where p_b and T_b are the pressure and temperature in the plenum chamber, respectively.

Similar to the above, the pressure at the quarter of the first leakage path can be regarded as the inlet pressure of the first half section of the first leakage path. For this part

$$m_{1+}=\frac{p_{l/4}^2-p_{out}^2}{48\mu RT_{l/4}}\frac{h_1^3 l}{H_1} \tag{8}$$

Besides, the leakage rate of the latter half section of the first leakage path can be calculated by the linear change of the square of the pressure at the outlet. The temperature shall also be changed to the outlet temperature. As a result, the mass flow through the second half of the first leakage path ($x/W>4$) is found by the temperature profile over the seal length x

$$m_{1-}=\int_{l/2}^{l}\frac{p_{4/l}^2-p_{out}^2}{24\mu RT(x)}\mathrm{d}x \tag{9}$$

Finally, the leakage mass can be expressed as

$$M=m_2+m_{1+}+m_{1-} \tag{10}$$

It can be seen from Table 1 that the decrease in the boundary layer thickness leads to an increase in the seal leakage rate. Meanwhile, compared with Steinetz's model, the modified model and numerical simulation results are in better agreement, which verifies the accuracy of the model. The error comes from the inhomogeneous pressure distribution in the first leakage path.

Table 1 Comparison of numerical calculation and predicted leakage rates under different boundary layer thicknesses

Boundary layer thickness	δ_{in}		
	$0.2W$	$0.6W$	$1.0W$
Numerical simulation/ (10^{-6} kg·s^{-1})	7.342	6.721	5.873
Modified model/ (10^{-6} kg·s^{-1})	7.561	6.992	5.916
Steneitz's model/ (10^{-6} kg·s^{-1})	4.924	4.924	4.924

4 Conclusions

The flow and leakage characteristics in the sealing cavity of the variable geometry hypersonic inlet are studied by numerical simulation.

(1) The flow in the seal chamber is a three-dimensional asymmetric open-type cavity flow under the influence of the boundary layer of the side plate. After being affected by the asymmetry, the pressure distribution of the two corresponding leakage channels on both sides of the cavity bottom shows that the pressure gradient at the inlet of the first leakage path is smoother than that of the second leakage path.

(2) As the thickness of the boundary layer increases, the vortices tend to squeeze toward the back wall of the cavity and the shear layer. Meanwhile, the pressure coefficient at the bottom of the chamber falls, thus reducing the inlet pressure of the leakage channel and leading to the decrease of the pressure difference between the inlet and outlet. Therefore, the sealing leakage is abated and the sealing performance is improved.

(3) According to the flow characteristics of the cavity configuration calculated in this paper, the existing seal model is modified, and the reliability of the model is verified by comparing it with the numerical simulation results.

References

[1] DUNLAP P, STEINETZ B, DEMANGE J. Further investigations of hypersonic engine seals: NASA/TM—2004-213188[R]. [S.l.]: NASA, 2004.

[2] DUNLAP P, STEINETZ B, DEMANGE J. High-temperature propulsion system structural seals for future space launch vehicles: NASA/TM—2004-212907[R]. [S.l.]: NASA, 2004.

[3] DUNLAP P, DEMANGE J, STEINETZ B. Performance evaluations of ceramic wafer seals[C]//Proceedings of the 42nd AIAA/ASME/SAE/ASEE Joint Propulsion Conference & Exhibit. Sacramento, California: AIAA, 2006.

[4] LI Yujie, LIU Yongbao, HE Xing. Numerical simulation for effects of clearance change of novel seal on aerodynamic performance of gas turbine[J]. Journal of Propulsion Technology, 2014, 36(8): 1170-1185. (in Chinese)

[5] CHEN Yaoxing, LI Zhigang, YAN Xin, et al. Investigations on the leakage characteristics and rotordynamic coefficients of labyrinth seal with tooth bending damage [J]. Journal of Xi'an Jiaotong University, 2018, 52(6): 157-164. (in Chinese)

[6] STEINETZ B. Evaluation of an innovative high temperature ceramic wafer seal for hypersonic engine applications: NASA TM-105556[R]. [S. l.]: NASA, 1992.

[7] KRISHNAMURTY K. Acoustic radiation from two-dimensional rectangular cutouts in aerodynamic surfaces: Technical Report CR-3487[R]. Washington DC, USA: NACA, 1955.

[8] ROSSITER J E. Wind-tunnel experiments on the flow over rectangular cavities at subsonic and transonic speeds[R]. [S.l.]: Royal Aircraft Establishment (RAE) Farnbough, 1966.

[9] LARCHEVÊQUE L, PIERRE SAGAUT P. Large-eddy simulation of a compressible flow in a three-dimensional open cavity at high Reynolds number[J]. Journal of Fluid Mechanics, 2004, 516: 265-301.

[10] LIU Jun, YANG Dangguo, WANG Xiansheng, et al. Effect of turbulent boundary layer thickness on a three-dimensional cavity flow[J]. Acta Aeronautica et Astronautica Sinica, 2016, 37(2): 465-483. (in Chinese)

[11] ZHANG X, EDWARDS J A. Computational analysis of unsteady supersonic cavity flows driven by thick shear layers[J]. Aeronautial Journal, 1988, 92(119): 365-374.

[12] JR STALLINGS R L, JR WILCOX F J. Experimental cavity pressure distribution at supersonic speeds: NASA TP-2683[R]. [S.l.]: NASA, 1987.

[13] LIU Chaoqun, WANG Yiqian, DUAN Zhiwei. New omega vortex identification method[J]. Science China Physics, Mechanics & Astronomy, 2016, 59(8): 1-9.

[14] DOLLING D S, PERNG S W, LEU Y L. An experimental study of passive control of hypersonic cavity flow oscillations: AFRL-SR-BL-TR-98-0240[R]. [S. l.]: Center for Aeromechancial Research, 1997.

[15] CROOK S D, LAU T, KELSO R M. Three-dimensional flow within shallow, narrow cavities[J]. Journal of Fluid Mechanics, 2013, 735: 587-612.

Acknowledgement This work was supported by the Opening Foundation of National State Key Laboratory of High Temperature Gas Dynamics (No.2021KF07).

Authors Mr. **XIA feng** is pursuing the M.S. degree at Nanjing University of Science and Technology. His main research interest is internal aerodynamics.

Dr. **SUN Bo** received the Ph.D. degree at Nanjing University of Aeronautics and Astronautics in 2007. Now he is an associate professor at Nanjing University of Science and Technology. His main research interest includes the internal aerodynamics and propulsion technology.

Author contributions Dr. **SUN Bo** designed the study and raised the idea. Mr. **XIA Feng** complied the models and wrote the manuscript. Dr. **YU Jianyi** contributed to data analysis, result interpretation and manuscript revision. Dr. **YUE Lianjie** contributed to the discussion and revision of the study. Mr. **GAO Yu** contributed to the discussion and background of the study. Dr. **DAI Chunliang** contributed to the design and discussion of the study. All authors commented on the manuscript draft and approved the submission.

Competing interests The authors declare no competing interests.

(Production Editor: XU Chengting)

高超声速可调进气道密封腔流动特性及泄漏规律研究

夏 枫[1]，孙 波[1]，于建一[2]，岳连捷[3]，高 钰[1]，代春良[1]

（1.南京理工大学机械工程学院，南京 210094，中国；2.北京机电工程总体设计部，北京 100190，中国；
3.高温气体动力学国家重点实验室，北京 100190，中国）

摘要：使用陶瓷晶片作为密封件对高超声速可调进气道进行密封时，密封腔内会出现受到侧板边界层影响的空腔流动。为了研究侧板边界层厚度对密封腔内流动特性和泄漏规律的影响，对不同来流边界层厚度下的密封腔模型进行了数值模拟。结果表明，密封腔内呈现出三维非对称的空腔流动结构，泄漏通道的入口压力也会受到非对称性的影响；随着边界层厚度的增加，空腔底部和密封入口处的压力降低。最后，根据空腔底板压力分布规律和泄漏通道中的流动特性，对现有的泄漏预测模型进行了修正。

关键词：可调进气道；陶瓷晶片密封；旋涡结构；泄漏率；三维非对称空腔流动